HgCdTe Long-Wave Infrared Photovoltaics for Directed Energy Applications

Robert Kaufman

Department of Electrical and Computer Engineering
University of Illinois at Urbana-Champaign, Urbana, Illinois, 61801, USA

(Completed 24 April 2022)

ABSTRACT

Free-space optical beam propagation in the long-wave infrared has been a field explored primarily for communication applications but may also provide utility in power-delivery, often termed as directed energy transfer. One critical issue that any of these systems must deal with is the absorption and perturbation of light in atmosphere. However, there are certain wavelength ranges, notably in the mid-wave and long-wave infrared (MWIR and LWIR), where the atmosphere is almost completely transmissive. With mature laser systems operating at LWIR wavelengths, such as quantum cascade lasers and CO_2 lasers, it may be practical to pair these sources with efficient LWIR photovoltaics (PV) to create directed energy systems for free-space power delivery. This could be utilized to network power supply between satellites or for powering electric drones and allowing continuous flight. This work presents a rudimentary design for a HgCdTe based LWIR photovoltaic to act as the receiver in such a system and utilizes Crosslight APSYS to perform electrical simulations. The design is optimized to convert the 10.6 μm optical emission of CO_2 lasers and multiple versions designed to operate a range of temperatures from 77 K to 300 K are investigated. Beyond this, the effects of incident power density is also explored. The best performing design and conditions produced a simulation result of 17.68% conversion efficiency at 77 K with 10 kW/m^2 incident optical power density. Finally, the limitations with using HgCdTe photodiodes as the power conversion device is reviewed such as its dependence on active cooling solutions.

I. INTRODUCTION AND MOTIVATION

From our cellphones to the satellites that enable their communications to our modes of transportation in the sky or on the ground, many modern technologies are untethered and mobile which introduces complexities in powering them. Traditionally, they are powered by local stores of energy, be it a battery or stored fuel, but this adds costs, weight, and still requires stationary recharging leading to additional downtime for the cases of vehicles. While there is equipment that utilize solar energy as their mobile source of energy, such as with satellites, they are not always exposed to the Sun, and this can limit usability and consistency of operation so often batteries are still required to store excess power to be used later [1]. An alternative solution to power these devices and in particular, vehicles, is through directed energy transfer. This involves the exchange of energy through free-space by delivering power through directed electromagnetic (EM) waves at some power converter at the receiving end. This is done through either lower-wavelength EM sources, such as radiofrequency (RF), or optical sources such as high-power lasers [2-6]. Preliminary research on both types of system have been examined with the electric systems typically used on smaller electronics where the transfer ranges are short and powers involved small versus the optical solutions being explored to power unmanned-air-vehicles (UAVs) or satellites over longer distances [2-6]. As an example, one of the better demonstrations of non-optical free-space energy transfer was 60 W being delivered over 2 meters at 40% medium transfer efficiency using a magnetic resonance coupling system [3]. In contrast, an early exploration of an optical directed energy system used a 5 kW fiber-laser to target a receiver at a distance of 3.2 km with 90% propagation efficiency [6]. This highlights the advantage the optical solutions have in both power density and range when compared to the lower frequency solutions. An illustration of a theoretical optical directed energy system is shown in Figure 1

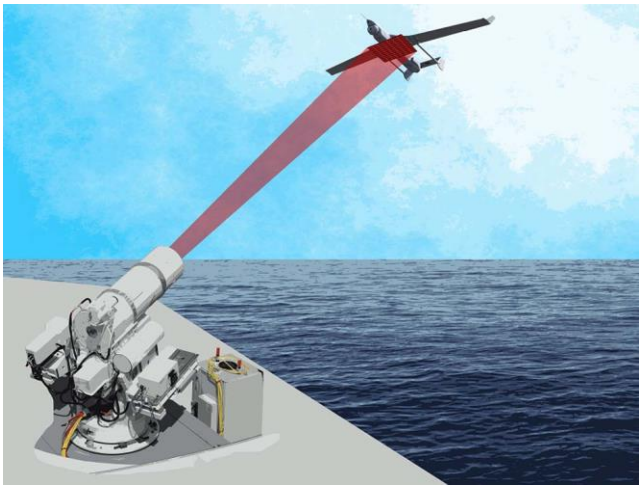

Figure 1. Illustration of hypothetical optical directed energy transfer system utilizing a high-power laser and photovoltaics on a UAV [5]

where the system parameters provided as an example include a 1 μm wavelength, 5 kW fiber-laser source that tracks and directs its beam to a specifically designed InGaAs photovoltaic (PV) with 40-50% conversion efficiency on the bottom of a UAV [5].

When designing an optical directed energy transfer system, the transmission wavelength is a crucial parameter as it can directly affect the effective propagation distance through atmosphere as well as inform the type of optical power converter that must be used. As can be seen in the atmospheric transmission spectrum shown in Figure 2, much of the optical spectrum is strongly absorbed by molecules in the atmosphere so it is important to select wavelengths in the high-transmissive windows [7]. One of these spectrally wider windows is in the long-wave infrared (LWIR) region of ardoun 8 to 12 μm which happens to correspond well with the common operating wavelength of the CO_2 laser at 10.6 μm, a well-developed and very high-power source. Another advantage of this higher-wavelength source, as compared to the ~ 1 μm fiber-lasers mentioned previously, is that wavelengths beyond 1.4 μm are considered "eye-safe" due to where the photons get absorbed in the eye [5]. Considerations of using CO_2 as a type of directed energy transfer source is noted as far back as a hypothetical analysis in 1976, but no fully developed systems at this wavelength are public [6]. However, in the tangential field of free-space optical communication, there has been significant investigations into using LWIR sources and photodiodes as detectors, typically based around the II-VI ternary HgCdTe [8-10]. Since the most likely blocker to such LWIR optical power delivery systems is difficulties in developing an efficient receiving photovoltaic, the advancements in HgCdTe photodiodes can be built upon to investigate its potential as a photovoltaic source when operated in the forward-active regime. It should be noted that so far, a major limitation of HgCdTe photodiodes is their poor performance above cryogenic temperatures, typically due to excess dark-current for detectors from the smaller material bandgap involved. Though that particular issue may be less relevant for a forward-

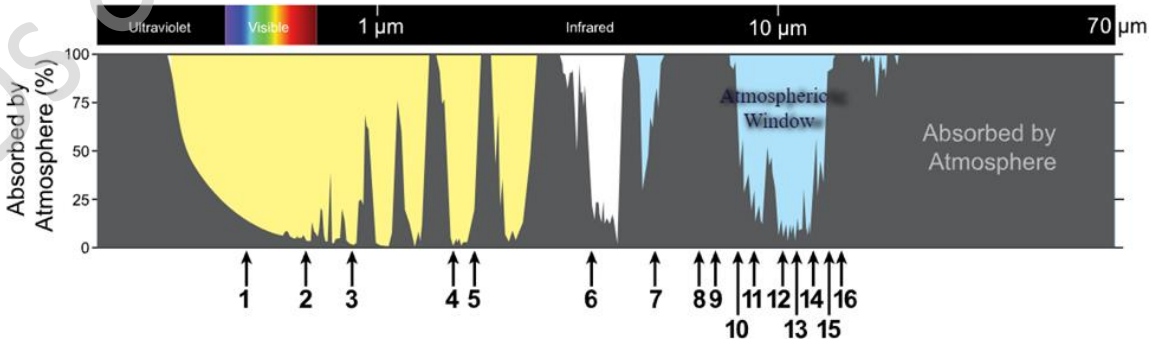

Figure 2. Absorption spectrum of Earth's atmosphere [7]

operated photovoltaic, other parameters could limit performance so it is important to investigate the temperature performance of the HgCdTe cells and is a key focus of this paper.

By combining the high-power, LWIR source of a CO_2 laser with a specifically designed HgCdTe photovoltaic, a more efficient and long-ranging directed energy transfer system can be envisioned. This system could provide solutions to long-range UAV powering as already being experimented with. This reduces UAV downtime which can be critical for keeping consistent information channels in defense situations. Another application that this could potentially provide is satellite power networks where excess power generated at lit-satellites or provided from the ground can power satellites in the dark. This can again increase up-time for certain tools and functions of these satellites and even reduce require battery capacity. The enhanced range, power densities, and directionality of optically-based directed energy systems enable these applications while the utilization of a LWIR optical source can help extend range and improve safety considerations. In order to determine the potential efficiency of such a system as well as ideal operating conditions and limitations, a rudimentary HgCdTe p-n photodiode is designed, structurally optimized, and simulated at different temperatures from 77 K to 300 K. The optimal design is then be simulated at different incident optical power as well due to the wide power range of LWIR laser options [6-7].

II. TECHNICAL BACKGROUND

Despite proposing to use a more exotic material than traditional photovoltaics for solar-cells, the HgCdTe LWIR photovoltaic is still a solid-state p-n junction photodiode and thus is governed by the same basic principles. By doping part of the device n-type and part of the device p-type, a p-n junction is created. At this junction, a depletion region forms where excess electrons from the n-side diffuse to the p-side and vise-versa creating a space-charge region and a built-in potential difference as seen in Figure 3. This formation creates a basic diode whereby applying a negative bias across the p-n terminals will further increase the total potential at the interface and make it difficult for any carriers to cross it and thus no current flows (until breakdown is reached). When forward biased, the built-in potential is acted against and the bands flatten, allowing current to pass between the two ends in the form of electrons and holes moving with the field. This basic operation gives rise to the simple, ideal diode equation:

$$I = I_0\left(\exp\left(\frac{qV}{mk_BT}\right) - 1\right) \qquad \text{(Eq. 1)}$$

When incident light falls on the diode, if the photon energy is greater than the bandgap, there is a chance that the photon is absorbed and an electron-hole pair is generated; an electron from the valence band is excited to the conduction band leaving a hold behind as depicted in the right depiction in Figure 3. If these excess carriers are able to reach the depletion-region of the device before recombining, they contribute a negative current referred to as photocurrent leading to the following simple diode equation:

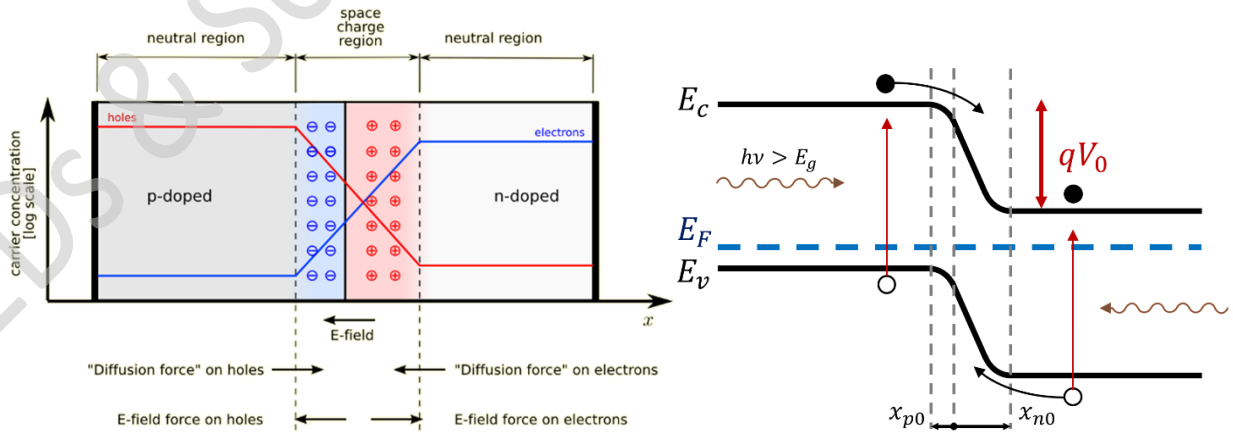

Figure 3. <u>Left:</u> Illustration of a p-n junction with carrier flow [11]. <u>Right:</u> Band-diagram of p-n junction exposed to incident photons

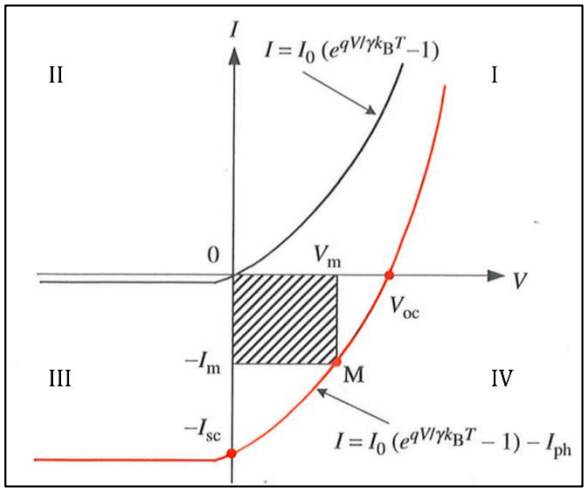

Figure 4. Plot of ideal photodiode curve when dark and when illuminated [12]

$$I = -I_{ph} + I_0 \left(\exp\left(\frac{qV}{mk_BT}\right) - 1 \right) \qquad \text{(Eq. 2)}$$

where I_{ph} is the photocurrent, and m is an ideality factor. As can be seen by this new equation, also plotted in Figure 4, the photocurrent shifts the diode curve down and for the purpose of solar-cells and photovoltaics, quadrant IV of the curve is of interest because there exists a negative current with a positive voltage. The electrical power consumed by some electrical device can be expressed as

$$P = IV \text{ (Eq. 3)}$$

In quadrant IV of the diode-curve, the negative current and positive voltage then indicates that the device is consuming "negative" power, thus power is generated. This is the mechanism a photovoltaic diode uses to convert optical power to electrical power.

To further investigate the performance of the HgCdTe photovoltaics, a deeper understanding and modelling of the interactions happening in this situation, primarily how recombination mechanisms affect the diode current. In order for optically generated carriers to actually contribute to the photocurrent, they must reach the built-in fields of the depletion region before recombining. The average distance a carrier can travel before recombining is called the diffusion length and is represented as L_n or L_p. This length is directly related to the lifetime of the carrier by the following:

$$L_n = \sqrt{D_n \tau_n} \qquad \text{(Eq. 4)}$$

Where D_n is the diffusion constant and τ_n is the carrier lifetime. This lifetime value comes from the combined recombination effects. In general, the three most common forms of recombination is Shockley-Read-Hall (SRH), direct-band, and Auger recombination. Shockley-Read-Hall recombination is a single-carrier event where an electron or hole gets trapped into some trap-level caused by impurities or other deep energy states. Direct-band recombination is when an electron in the conduction band recombines and fills a hole in the valence band. Auger is a 3-particle event where an electron-hole pair will recombine, but an exchange of momentum will also occur and cause the shift in energy of another electron or hole. Combined, these three mechanisms make up the ABC model of recombination that is as follows assuming high-level injection where Δn represents the excess carriers:

$$R(\Delta n) \approx A \cdot \Delta n + B \cdot \Delta n^2 + C \cdot \Delta n^3 \qquad \text{(Eq. 5)}$$

This combined recombination rate represents the change in excess charges in the semiconductor and thus is inversely related to the total lifetime, τ_n:

$$-R(\Delta n) \approx \frac{\Delta n}{\tau_n} \quad \text{(Eq. 6)}$$

This means, that the higher the recombination rate is, the lower the carrier lifetime is and subsequently the shorter the diffusion length is. This will negatively affect the photocurrent that is generated from absorbed photons and so for an efficient photovoltaic, recombination effects should be minimized.

Beyond recombination minimization, since semiconductor devices are not ideal and often feature a variety of defects from imperfect growths, occurrences like shunt paths and series resistance should be considered. While not a focus of the simulations for the HgCdTe photovoltaics, it is still important to understand how these elements can affect a real-world version of the device. A common electrical model of a photovoltaic photodiode to account for these components is to separate the photocurrent as a pure current source, include the diode in parallel and opposite, include a parallel shunt resistance, and then finally a series resistance as per Figure 5. This leads to a more complete diode equation:

$$I = -I_{ph} + I_0\left(\exp\left(\frac{q(V-IR_S}{mk_BT}\right) - 1\right) + \frac{V+IR_S}{R_{SH}} \quad \text{(Eq. 7)}$$

Both intuitively and through this equation, it can be seen that reducing these undesired resistances will help improve the efficiency of power conversion. Shunt paths further detract from the generated photocurrent while series resistance reduces the operating voltage at some current.

When evaluating the HgCdTe photovoltaic designs, the primary metric considered is total power conversion efficiency which is simply:

$$\eta = \frac{P_{max}}{P_{opt}} = \frac{I_{max}V_{max}}{P_{opt}} \quad \text{(Eq. 8)}$$

Where I_{max} and V_{max} are the current and voltages that produce the maximum output power and P_{opt} is the incident optical power; an example of these values are indicated on Figure 4 at point *M*. While this gives the real-world performance of the cell, other metrics can be useful to inform trade-offs and areas for improvement. The open-circuit voltage, V_{oc}, and short-circuit current, I_{sc}, is simple the voltage at 0 A of current and the current at 0 V respectively. Given that power is the product of current and voltage, these are useful for estimating the peak power potential of the cell though since no diode is perfectly ideal, the true max power will always be smaller. The ratio from the actual max power to this "ideal" standard is called the fill-factor and is given by:

$$FF = \frac{P_{max}}{V_{oc}I_{sc}} = \frac{I_{max}V_{max}}{V_{oc}I_{sc}} \quad \text{(Eq. 9)}$$

One example of where these metrics are useful is increasing generated power output by increasing the open-circuit voltage. Since the turn-on voltage of diode is roughly related to the bandgap energy in eV.
to increase V_{oc}, the design bandgap of the material can be increased across it or more in certain regions.

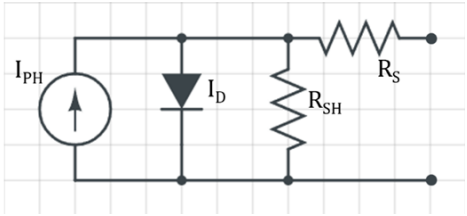

Figure 5. Circuit model of a photodiode including series resistance and a shunt path

III. LWIR PHOTOVOLTAIC DESIGN

To analyze the performance and limitations of the HgCdTe photovoltaic, device designs were modelled to be simulated in Crosslight APSYS, a finite-element physical semiconductor simulator. The first step, before building out the physical design was to ensure that the material parameter file was accurate. While a HgCdTe material file existed, some conventions and models were outdated so a custom one was made based off the first. Of primary interest was accurate modelling of bandgap, absorption, and recombination rates for different compositions, temperatures, and incident optical wavelengths. The main revisions included updating the effective electron mass, the absorption below and above gap, the intrinsic carrier concentration, electron affinity and relative permittivity using sources from literature [13-18]. Details of all sources and edits can be found commented in the provided material file "HgCdTe2022.mac".

One of the first considerations for the design was to make sure it was reasonably physical to grow and thus ranges for doping and composition are only used if it has been shown in literature. HgCdTe crystals have been grown by a variety of methods including liquid-phase epitaxy (LPE), metal-organic chemical vapor deposition (MOCVD), and molecular beam epitaxy (MBE) on a variety of substrates including Si and CdZnTe [19]. For the purpose of this simulation experiment, growth substrates are not considered although for real devices, it is an important criterion in order to limit defects and keep unwanted recombination effects reduced. Donor doping utilizes Group-III and VII elements with the most common sources being indium and iodine [19]. For acceptor doping, Group-I and V elements are used such as lithium and arsenic [19]. The concentration range for these dopants have been experimentally shown successfully up to 10^{21} cm^{-3} for donors and up to 10^{20} cm^{-3} for acceptors and thus, this will be the upper-limit considered in the designs presented here [19].

The basic HgCdTe photovoltaic started as a simple p-i-n diode featuring two junction regions to increase the area to produce absorb photons and produce generate productive carrier pairs. Due to the complexities of HgCdTe at higher temperatures, the design was optimized first for 77 K operation before manually tweaking it for higher temperature operation. The next major parameter to tune was the ternary composition with consideration primarily given to the bandgap which can be expressed by [15]:

$$E_g(x,T) = -0.302 + 1.93x - 0.81x^2 + 0.832x^3 + 5.35 \times 10^{-4}(1-2x)T \qquad \text{(Eq. 10)}$$

As noted earlier, it is desirable to keep the bandgap large in-order to keep the open-circuit voltage larger, but if it the bandgap is too large, the 10.6 μm photons will not be absorbed. For the 10.6 CO_2 laser, each photon carries an energy of 0.117 eV which sets the cut-off energy that the bandgap must be below. Also, the absorption rates of HgCdTe at 10.6 μm versus bandgap was referenced to find which range will reasonably capture the light. As can be seen by the plot in Figure 6, a HgCdTe composition with bandgaps around x=0.16 to 0.23 provide strong absorption. This gave a starting point around $Hg_{0.8}Cd_{0.2}Te$ (x=0.2 for

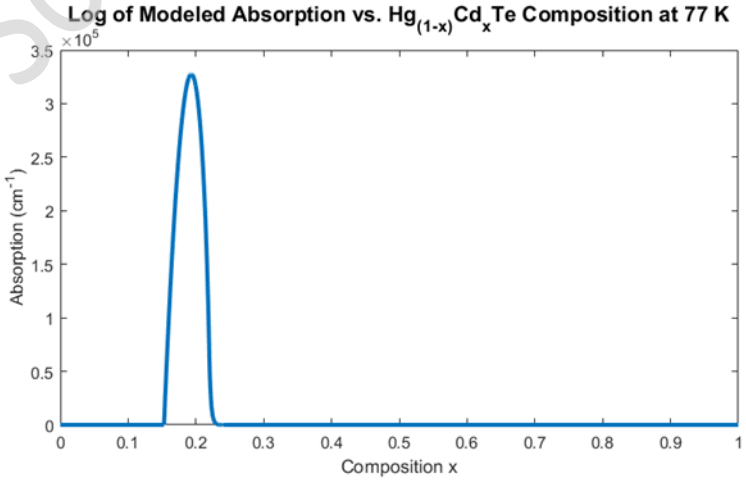

Figure 6. Modeled absorption of HgCdTe at 77 K versus composition for a 10.6 μm photon [13-14]

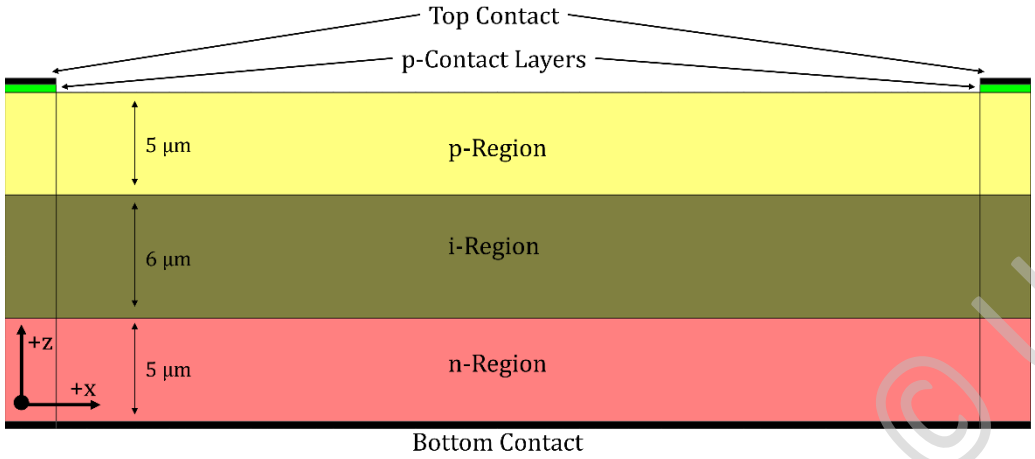

Figure 7. HgCdTe Photovoltaic physical device design

$Hg_{(1-x)}Cd_xTe$) and further tweaking found the best performance for the 77 K-designed PV at x=0.215 with a bandgap of 0.1073 eV. As part of this tweaking process, donor doping and acceptor doping levels were optimized. Finally, as an attempt to push efficiency just a bit further without major modifications, a small contact region was added above the p-type layer just under the contacts. Here, the composition was shifted higher to x=0.25 in-order to increase the bandgap to 0.1637 eV and increase the open-circuit voltage, the effects of which will be compared in the simulations. The final base design and its band structure is shown in Figure 7 and Figure 8 with the parameters used listed in Table 1.

Main Composition	x=0.215	**p-Contact Composition**	x=0.25
p-Doping	$1x10^{17}$ cm^{-3}	**p-Thickness**	5 µm
n-Doping	$1x10^{16}$ cm^{-3}	**n-Thickness**	5 µm
i-Thickness	6 µm	**p-Contact Thickness**	0.1 µm
Total Width	50 µm	**Top Contact Width**	2.5 µm each

Table 1. Design parameters for HgCdTe LWIR photovoltaic

One unique characteristic of $Hg_{(1-x)}Cd_xTe$ is that for compositions below 50% CdTe (x < 0.5), the bandgap behaves the opposite of trend found in III-V semiconductors as noted by Varshni's Equation; usually, bandgap decreases as temperature increase but for $Hg_{>0.5}Cd_{<0.5}Te$, the bandgap actually increases with temperature [15]. One particular challenge with this, since the designed composition has a bandgap close to the design wavelength energy, is that for higher temperature operation, the bandgap of the absorbing regions quickly grows too large and the photovoltaic is now transparent to the low-energy LWIR photons and thus no photocurrent can be generated. Because of this, the decision was made to make a new, specific

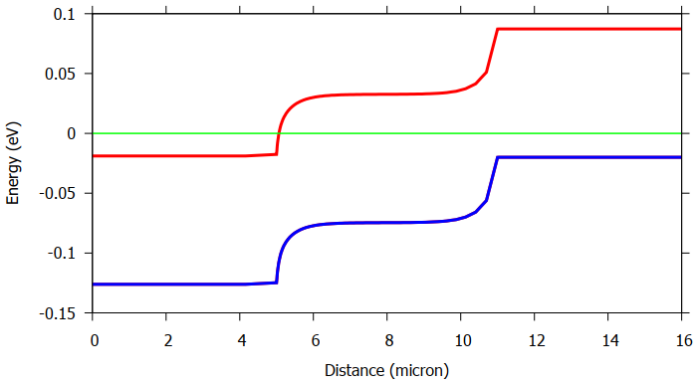

Figure 8. Band-diagram of HgCdTe Photovoltaic; 0 µm is at the bottom contact

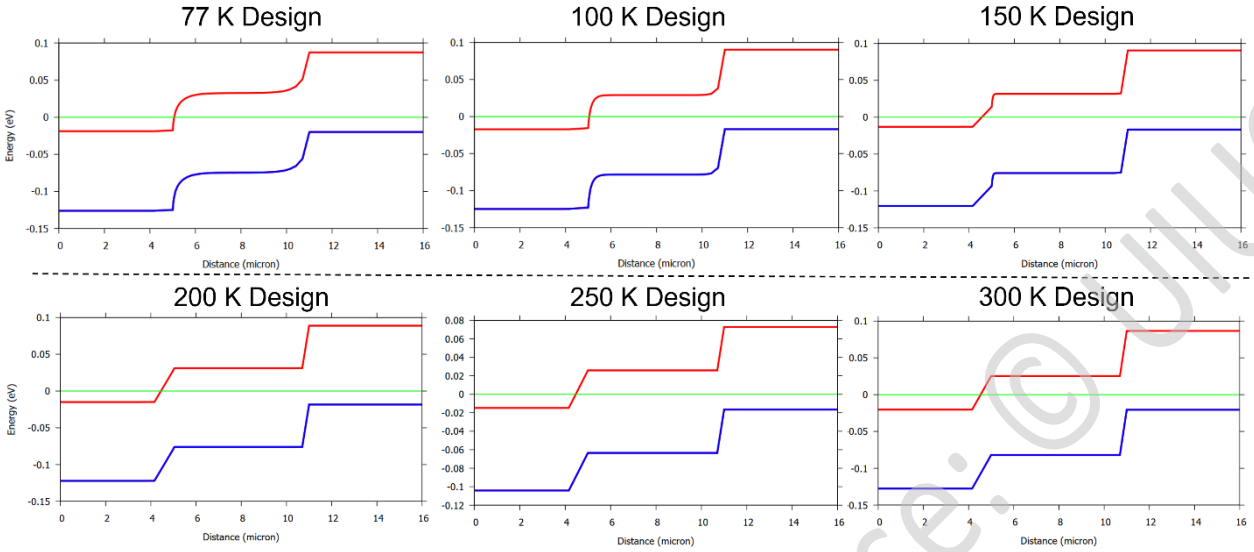

Figure 9. Comparison of band-diagrams for each of the different temperature HgCdTe PV designs

design for a range of increasing temperatures. The temperature values designed for were 77 K, 100 K, 150 K, 200 K, 250 K, and 300 K. First, new compositions were found to match the bandgaps of each layer to that in the 77 K design and then the doping was tweaked to try and match the band structure. The composition was found by solving Eq. 10 for each temperature and a bandgap of 0.1073 eV for the absorbing region. All the final designs' parameters are listed below in Table 2 along with their respective band-structures in Figure 9.

Design	**Main Composition**	**p-Contact Composition**	**p-Doping (cm^{-3})**	**i-Doping (cm^{-3})** *p-type*	**n-Doping (cm^{-3})**
77 K	0.2150	0.2500	1.0×10^{17}	0	1.0×10^{16}
100 K	0.2106	0.2461	5.0×10^{27}	1.0×10^{14}	1.0×10^{16}
150 K	0.2006	0.2372	2.0×10^{18}	1.0×10^{16}	1.0×10^{16}
200 K	0.1898	0.2276	4.0×10^{18}	7.0×10^{16}	1.0×10^{16}
250 K	0.1784	0.2174	8.0×10^{18}	5.0×10^{17}	5.0×10^{16} (p-type)
300 K	0.1661	0.2064	1.0×10^{19}	5.0×10^{17}	5.0×10^{16} (p-type)

Table 2. Design differences between LWIR PVs made for specific temperature operation

IV. EXPERIMENTS, SIMULATION RESULTS, AND ANALYSIS

A. BASIC DESIGN OPTIMIZATION AT 77 K

To demonstrate minimum feasibility, the first simulation experiment investigates the 77 K designed device. This is done by taking dark and illuminated forward-biased IV curves with an incident power of 10 kW/m^2 at 10.6 μm to approximate the narrow spectral width of a laser. Naturally, this device was simulated at 77 K. Using the Crosslight APSYS software, an electrical and optical device simulation was run on the design in Figure 7 by taking a dark voltage sweep from 0 to 0.1 V forward-bias. The 10.6 μm light incident on top of the device was then ramped to full power and the same voltage-sweep was performed. For the purpose of investigating the base device performance, no coatings were considered, and an 100% optical transmission was enforced accompanied by an 100% back-reflection to present the most ideal condition; this setting is held constant in all the simulations in this paper. The IV behavior is shown in Figure 10; from the left, full-range curve, it can be seen that the 77 K HgCdTe PV design does indeed behave like a diode with an exponential forward-bias profile. In addition, when illuminated, a photovoltaic effect is observed and a photocurrent of 5.62 A/cm^2 is generated. This is better seen in the right plot of Figure 10 where the

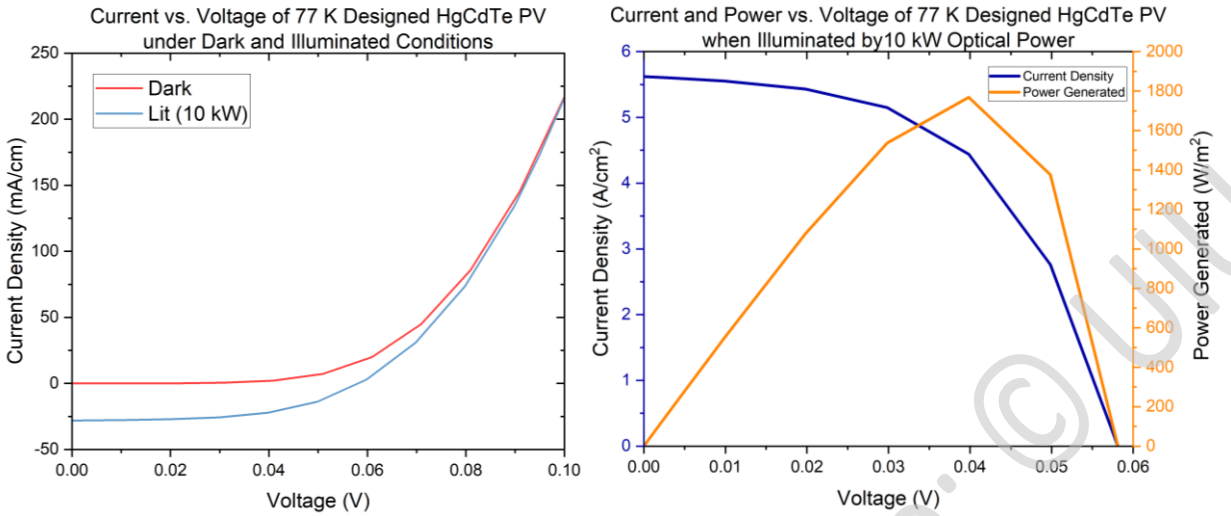

Figure 10. Left: IV plot of 77 K PV when Dark and Illuminated. Right: Quadrant IV of 77 K diode curve with generated power plotted on the right axis

quadrant IV region is enhanced and power is plotted along with current. The device has a short-circuit current-density of 5.62 A/cm^2 and an open-circuit voltage of 0.0581 V with a maximum power generation of 1768 W/m^2 for a 17.68% total efficiency. All performance metrics are stated below in Table 3. What is clear from this first simulation is that HgCdTe is a viable candidate to a construct a LWIR PV from with even a rudimentary design delivering conversion efficiencies nearing 20%.

Eff. (%)	P_{max} (W/m^2)	J_{max} (A/cm^2)	V_{max} (V)	J_{sc} (A/cm^2)	V_{oc} (V)	FF (%)
17.68 %	1768	4.44	3.98 x10^{-2}	5.62	5.81 x10^{-2}	54.1 %

Table 3.Performance metrics for 77 K HgCdTe PV when illuminated with 10 kW/m^2

Next, to investigate one of the small design improvements, the addition of the higher bandgap p-contact layer, the device is simulated with and without it at 77 K. The device structure without the p-contact region is the same as in Figure 7 except without the thin 100 nm "p-Contact Layers" present. The expectation by including a high-composition interface layer, which has a bandgap of 0.1635 eV compared to the 0.1073 eV of the main region, is that the open-circuit voltage is slightly extended and more power is generated that way. Performing the same sweeps as on the original design, more dark and illuminated simulations are performed. Figure 11 compares the power generation the results in area-of-interest with Table 4 listing the performance metrics. Indeed, the open-circuit voltage extended from 0.0562 V to 0.0581 V but another contributing factor was the increase in short-circuit current as well. One possible explanation for this is that it technically forms another small junction and increases the total depletion area of the device and thus allows more of the generated carriers to contribute to the photocurrent. The small added layer improves the efficiency of the LWIR photovoltaic through the increase of open-circuit voltage and thus was included in all further investigated designs.

Design	Eff. (%)	P_{max} (W/m^2)	J_{max} (A/cm^2)	V_{max} (V)	J_{sc} (A/cm^2)	V_{oc} (V)	FF (%)
No Contact	16.45	1645	4.13	3.98 x10^{-2}	5.30	5.62 x10^{-2}	55.2
Contact	17.68	1768	4.44	3.98 x10^{-2}	5.62	5.81 x10^{-2}	54.1

Table 4. Comparison of performance between LWIR PV design with and without the p-contact layer

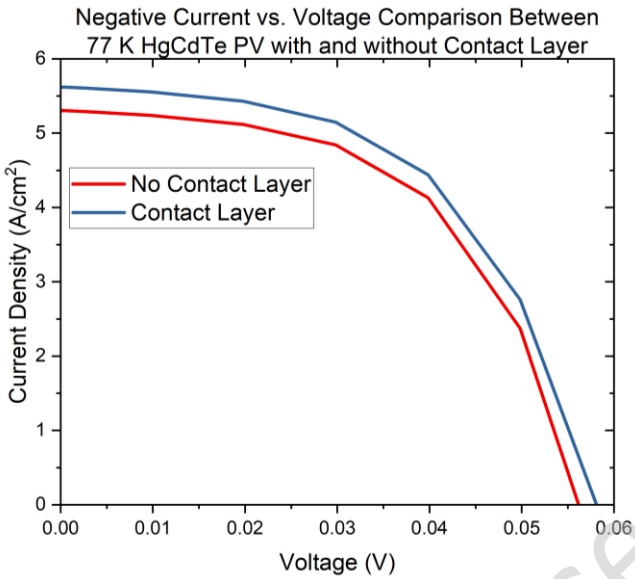

Figure 11. Comparison of illuminated IV between HgCdTe PV design with and without a p-contact layer

B. COMPARISON OF SPECIFIC TEMPERATURE DESIGNS

The next simulation experiment is to compare the HgCdTe performance versus temperature. As mentioned in design, at each temperature, a specific design was made with slightly different composition and doping concentrations to try and equate the band profiles and most important, bandgap. Each device is simulated at their design temperature and the forward-bias diode curves are taken under dark and illuminated conditions. The incident optical light is set to a static 10.6 μm source with a total power of 100 kW in order to reach observable current generation in all situations. The simulation results are depicted below in Figure 12 and performance metrics notes in Table 5.

Design	**Eff. (%)**	**P_{max} (W/m^2)**	**J_{max} (A/cm^2)**	**V_{max} (V)**	**J_{sc} (A/cm^2)**	**V_{oc} (V)**	**FF (%)**
77 K	11.83	11830	27.0	4.38×10^{-2}	45.7	7.49×10^{-2}	34.5
100 K	10.92	10920	27.4	3.98×10^{-2}	40.8	5.97×10^{-2}	44.8
150 K	1.727	1727	15.6	1.10×10^{-2}	26.3	2.12×10^{-2}	30.9
200 K	0.08779	87.79	6.56	1.34×10^{-3}	12.4	2.79×10^{-3}	25.4
250 K	8.253×10^{-5}	8.253×10^{-2}	0.396	2.09×10^{-5}	0.792	4.17×10^{-5}	25.0
300 K	7.293×10^{-4}	7.293×10^{-1}	1.36	5.37×10^{-5}	2.71	1.07×10^{-4}	25.0

Table 5. Performance metrics for each specific temperature design when illuminated with 100 kW/m^2

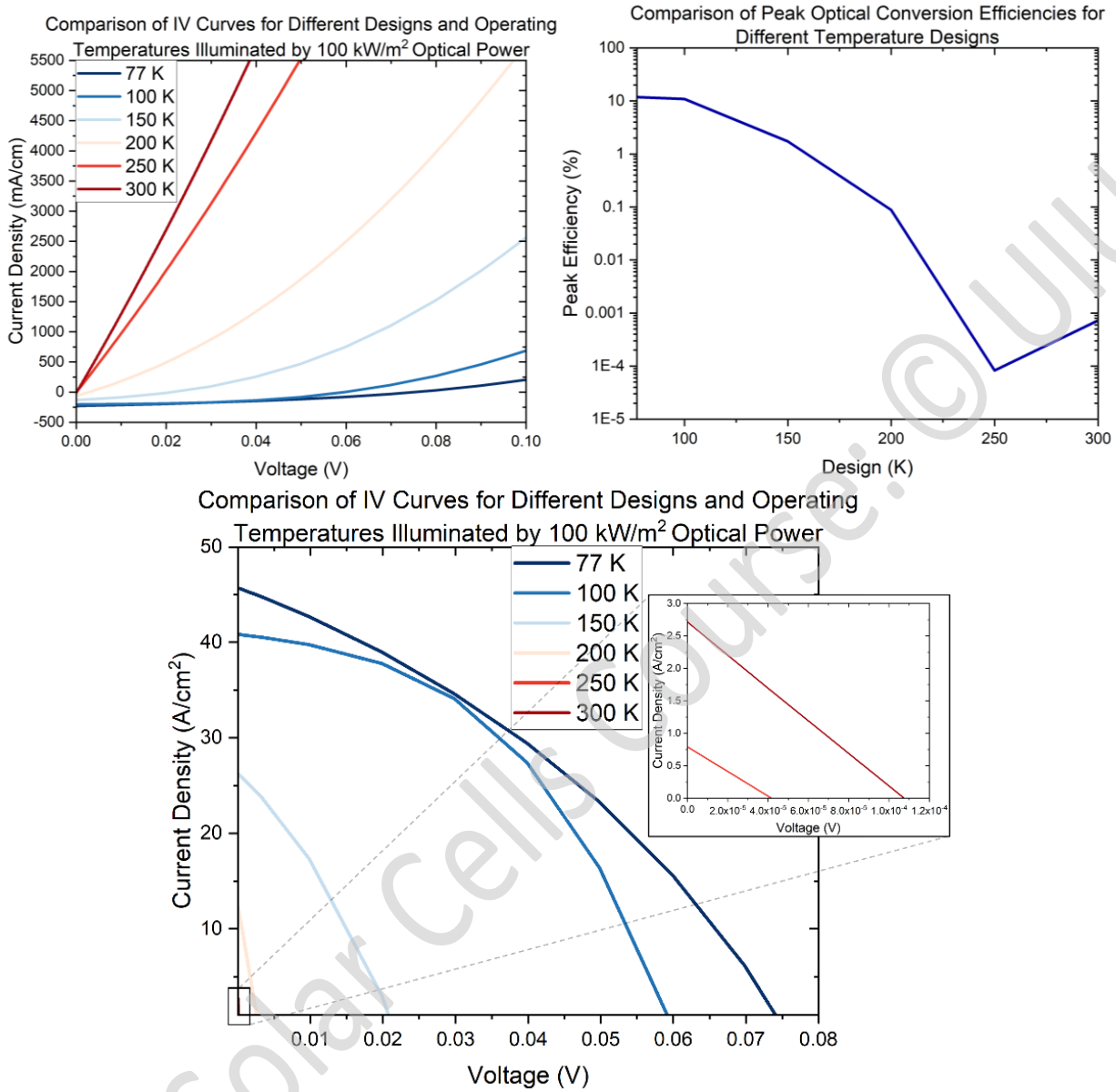

Figure 12. <u>Top-Left:</u> Illuminated IV plot for each specific temperature design operated at their designed temperature. <u>Top-Right:</u> Log-plot of peak efficiency versus temperature design. <u>Bottom:</u> Quadrant IV illuminated diode curve for each temperature design

The simulation results reaffirm the notion that HgCdTe is a difficult material to utilize above cryogenic temperatures with the 77 K design converting the incident light most efficiently while the 300 K design struggles to convert much power at all with only a 7.293×10^{-4} % efficiency. The most efficient device was the 77 K design with an 11.83% efficiency and the 100 K design not far behind at 10.92%. A couple of mechanisms can help to explain this trend: diode trends with increased temperature and increased recombination. Increasing temperature plays the role of broadening the exponential diode curve as can be extracted from Eq. 2; this will have the effect of potentially extending V_{oc}, which would be positive, but also decreasing the fill-factor which is apparent in the results as the fill-factor trends towards 25% with increasing temperature (which is the fill-factor of a straight line). Physically, this can be thought of as more thermal energy existing in the carriers and increasing the probability they can move over the junction barrier. This is especially severe for the HgCdTe-based PVs since the bandgap is so small to start with at only 0.1073 eV, effectively turning the diode into a resistor at high temperatures.

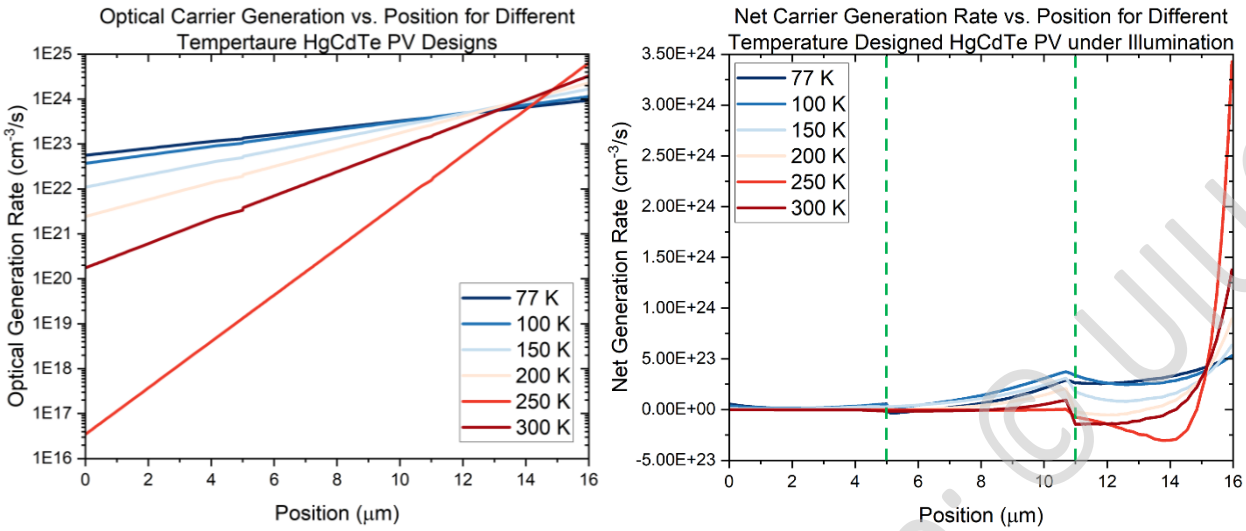

Figure 13. <u>Left:</u> Log-plot of optical carrier generation vs. position in the device for different temperature designs. <u>Right:</u> Net carrier generation (optical carrier generation – recombination) vs. position.

Beyond the unavoidable diode physics (at least for the simple design presented), the material parameters of recombination and absorption play a role as well. Firstly, the absorption for HgCdTe increases with temperature for some fixed bandgap [13-14]. This has the effect of the top-region of the device generating more electron-hole-pairs but at the sacrifice of carrier generation further into the device. This trend is viewable in the spatial carrier distribution shown on the left plot of Figure 13; as temperature increases, the carriers are more and more preferentially generated at the surface (16 μm) compared to the bottom of the device (0 μm). This could pose saturation issues and does not as efficiently utilize the two junctions present in the structure. Combine this with the increased recombination seen as temperature increases, and the higher absorption may be a detriment for this device design. To visualize the net excess carrier across the device, the three primary recombination mechanisms, Shockley-Reed-Hall, Auger, and radiative, were measured for each simulation and subtracted from the optically generated carrier rate. This is plotted in Figure 13 and as can be seen at higher temperatures, despite generating more carriers at the surface, the larger recombination rate absorbs almost all the generated carriers before the second junction. As noted earlier, higher recombination leads to decrease of carrier lifetime, reduced diffusion length, and thus reduced generated photocurrent. Each of these factors contribute to severely limit the performance for the HgCdTe photovoltaic at higher temperatures and reaffirms that temperature is a very limiting factor on the practicality of such material choice.

C. TEMPERATURE EFFECT ON CONSTANT DESIGN PERFORMANCE

Despite the poor performance of the 300 K design, due to the inverse Varshni relation of its $Hg_{0.834}Cd_{0.166}Te$ composition, its bandgap will actually decrease at lower temperatures, so it will still provide substantial absorption of 10.6 μm photons across lower temperatures. This allows it to be used to gather a rough trend of how temperature affects a constant HgCdTe-based PV design. A similar simulation and metric extraction is run on the 300 K-designed LWIR photodiode but at temperatures of 77 K, 100 K, 150 K, 200 K, and 250 K in order to compare its performance with cells specifically designed for those temperatures. Figure 14 shows the quadrant IV current-voltage curves on the left and the peak efficiency of the cell on the right plot with Table 6 displaying all the parameters. It is apparent that the diode behavior and continuous to be poor at all temperatures with the linear fill-factor of 25% being present on all samples. Beyond that, the 300 K design performs worse than all the specific temperature designs which is expected given that the increasing bandgap and decreasing intrinsic carrier concentration will also elements such as total light absorbed (and thus carrier generation), recombination rates, and junction widths. When analyzing

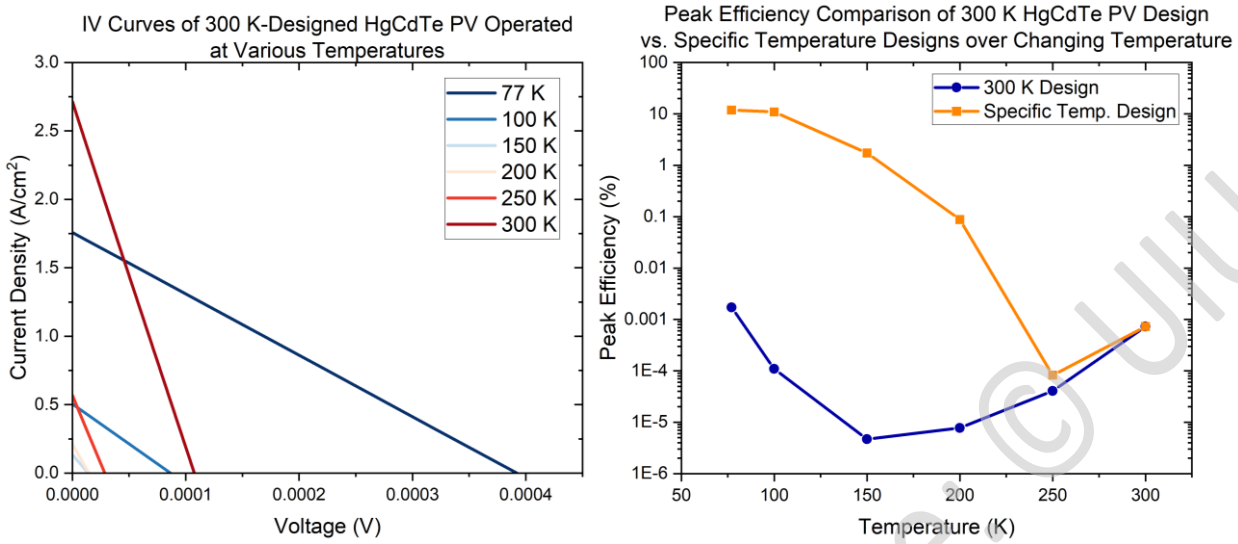

Figure 14. Left: Quadrant IV current-voltage curve for 300 K LWIR PV design when operated at other temperatures. Right: Log-plot of peak conversion efficiency for 300 K LWIR PV operated at other temperatures.

just the trend of the 300 K design versus temperature, it is interesting to see how efficiency initial starts to drop as temperature is decreased but then rises again at the 77 K and 100 K with larger voltages being the primary driver of power increase. This experiment seems to indicate that once again, an efficient LWIR HgCdTe PV will likely have to operate at cryogenic temperatures to be effective.

Temp. (K)	Eff. (%)	P_{max} (W/m^2)	J_{max} (A/cm^2)	V_{max} (V)	J_{sc} (A/cm^2)	V_{oc} (V)	FF (%)
77	1.723×10^{-3}	1.723	0.879	1.96×10^{-4}	1.76	3.92×10^{-4}	25.0
100	1.093×10^{-4}	0.1093	0.252	4.33×10^{-5}	0.505	8.66×10^{-5}	25.0
150	4.695×10^{-6}	4.695×10^{-3}	6.71×10^{-2}	7.00×10^{-6}	0.134	1.40×10^{-5}	25.0
200	7.715×10^{-6}	7.715×10^{-3}	0.105	7.32×10^{-6}	0.211	1.46×10^{-5}	25.0
250	4.042×10^{-5}	4.042×10^{-2}	0.284	1.42×10^{-5}	0.568	2.85×10^{-5}	25.0
300	7.293×10^{-4}	7.293×10^{-1}	1.36	5.37×10^{-5}	2.71	1.07×10^{-4}	25.0

Table 6. Performance metrics for 300 K LWIR PV design being operated at different temperatures with 100 kW/m^2 incident optical power

D. EFFECT OF INCIDENT POWER LEVEL ON PERFORMANCE

With the 77 K design cemented as the most efficient of the investigated, despite its need for active cooling, it will be used a further exploration on efficiency versus incident power since a wide-range of power options exists for CO_2 lasers [5-6]. To investigate this, a lit simulation with a similar voltage sweep is ran for the 77 K designed HgCdTe PV with increasing incident powers (in factors of 10) from 10 W/m^2 to 100 kW/m^2. The intent is to find the approximate magnitude range of incident power where the LWIR PVs operate most efficiently without being saturated. The IV curves for each power are shown below in the left plot of Figure 15 with their efficiency trend plotted on the right; Table 7 lists all the performance metrics. From this data, the incident power most efficiently converted was 10 kW/m^2 with an efficiency of 17.68%. That said, due to the decreasing fill-factor from 56.7 to 54.1%, there may be a more optimal power between 1 kW/m^2 and 10 kW/m^2 where the diode curve maintains a sharper turn-on. At 100 kW/m^2, the efficiency drops off to below that of 1 kW/m^2, down to 11.83% as the device is saturated. The massive amount of excess carrier generation likely deforms the band-structure to a degree such that the diode performance suffers; a comparison of the band-structure under illumination for the 1 kW/m^2 test and the

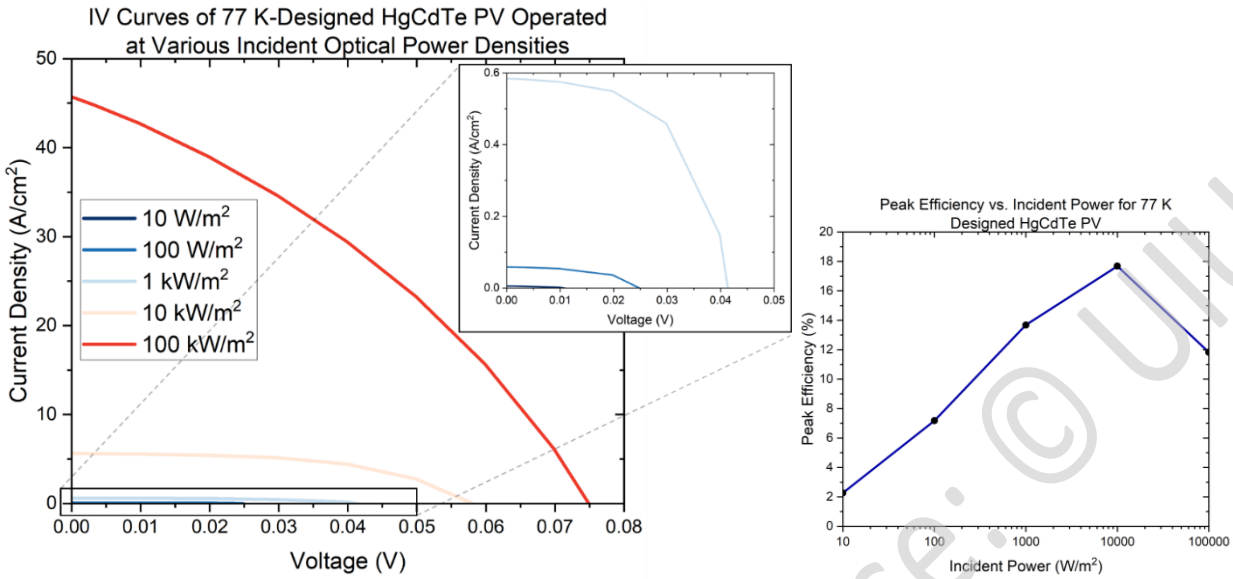

Figure 15. <u>Left:</u> Quadrant IV illuminated diode curve of the 77 K LWIR PV under different incident powers. <u>Right:</u> Peak efficiency vs. incident power.

100 kW/m^2 is shown in Figure 16. This simulation did not consider the heating that would occur for such high incident power densities and given the poor performance of the HgCdTe PVs with increasing temperature, the 100 kW/m^2 test would likely perform even worse.

Inc. P (W/m^2)	Eff. (%)	P_{max} (W/m^2)	J_{max} (A/cm^2)	V_{max} (V)	J_{sc} (A/cm^2)	V_{oc} (V)	FF (%)
10	2.271	0.2271	3.39 x10^{-3}	6.69 x10^{-3}	5.87 x10^{-3}	1.09 x10^{-2}	35.4
100	7.177	7.177	3.64 x10^{-2}	1.97 x10^{-2}	5.87 x10^{-2}	2.48 x10^{-2}	49.2
1000	13.68	136.8	0.460	2.98 x10^{-2}	0.584	4.14 x10^{-2}	56.7
10000	17.68	1768	4.44	3.98 x10^{-2}	5.62	5.81 x10^{-2}	54.1
100000	11.83	11830	27.0	4.38 x10^{-2}	45.7	7.49 x10^{-2}	34.5

Table 7. Performance metrics of the 77 K LWIR PV under different incident powers

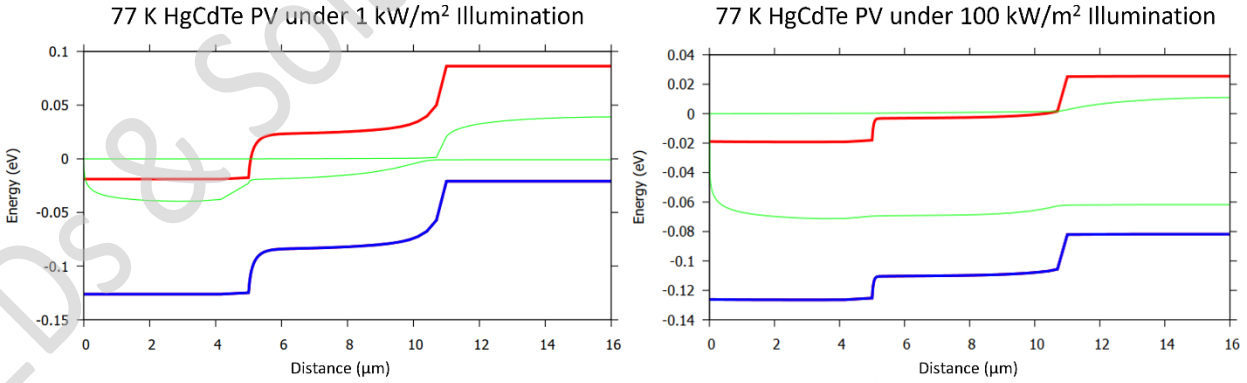

Figure 16. <u>Left:</u> Band-diagram of 77 K LWIR PV under 1 kW/m^2 illumination. <u>Right:</u> Band-diagram of same device under 100 kW/m^2.

V. CONCLUSION

Directed energy transfer systems can help to improve the uptime and costs to operate certain mobile devices, such as UAVs or satellites. High-power optical-based systems shows the most promise for their ability to direct high levels of power over kilometers of range. While near infrared (NIR) systems have been investigated, a system designed for long-wave infrared beams may prove to be beneficial in extending the range and reliability due to improved atmospheric transmission characteristics. On this merit, this paper sought to develop a rudimentary design of a LWIR photovoltaic to act as the power converting receiver. The design focused on the operating properties of a HgCdTe photodiode optimized for converting the high-power 10.6 μm emissions of a CO_2 laser. Through simulations using Crosslight APSYS, it was shown that the best performing design operated at a temperature of 77 K and incident with 10 kW/m^2 of optical power could convert with an efficiency of 17.68%. It was also shown that as temperature increases, the material parameters much be carefully chosen since bandgap of $Hg_{>0.5}Cd_{<0.5}Te$ increases with temperature and so unique specific designs should be made for a narrow temperature range. Rough replications of the 77 K design at high temperatures showed that even when accounting for the bandgap change, the efficiency of the photovoltaics is drastically diminished with the 300 K operating design producing an efficiency of $7.293x10^{-4}$ %. Finally, the effect of incident power on the HgCdTe photovoltaic efficiency was simulated since CO_2 can exhibit a large range of powers and through optics, power densities. Ignoring heating effects, 10 kW/m^2 of incident power provided the most efficient operating condition with the 17.68% conversion percentage as mentioned above. The saturating of the cell at the higher power density of 100 kW/m^2 reduced the efficiency to 11.83%.

While a functional HgCdTe photovoltaic was shown through simulations with a decent conversion efficiency, there is still room for improvements and areas of concern for the practicality of such a device. More advanced designs may be able to improve the collection efficiency and include structures to improve the diode behavior even further. The small bandgap required for LWIR absorption limits how quickly the diode will turn-on and the open-circuit voltage that can be obtained. This second consideration can also cause some issues in operation given that the best performing simulated PV had a V_{oc} of 0.0581 V which is over 10x smaller than something like a silicon cell. Accounting for just this voltage would require finer electronic control and may be impractical to pair directly to some systems though placing cells in series can help mitigate this issue. The bigger issue for these HgCdTe PVs is their poor temperature performance. With practically needing to be at cryogenic temperatures, they will require active cooling which consumes power and will reduce the net efficiency of the system. Room-temperature HgCdTe photodiodes to act has detectors have been researched, so it may be possible to expand on those advancements to make improvements to this simple HgCdTe PV [8]. If thermal concerns are able to be addressed, then one potential future improvement to the cell would be to grow it on a silicon wafer that is then processed to act as a traditional solar-cell effectively creating a LWIR and NIR tandem cell. This would involve a careful spatial design to ease processing and a tunnel-junction to connect the two cells. If possible, this could enable further space and weight savings allowing both solar powering as well as LWIR directed energy transfer on the same device.

VI. REFERENCES

[1] Hill, Carole A. "Satellite battery technology—A tutorial and overview." *IEEE Aerospace and Electronic Systems Magazine* 26.6 (2011): 38-43. https://doi.org/10.1109/MAES.2011.5936184

[2] Xie, Liguang, et al. "Wireless power transfer and applications to sensor networks." *IEEE Wireless Communications* 20.4 (2013): 140-145. https://doi.org/10.1109/MWC.2013.6590061

[3] Kurs, Andre, et al. "Wireless power transfer via strongly coupled magnetic resonances." *science* 317.5834 (2007): 83-86. https://doi.org/10.1126/science.1143254

[4] Li, Siqi, and Chunting Chris Mi. "Wireless power transfer for electric vehicle applications." *IEEE journal of emerging and selected topics in power electronics* 3.1 (2014): 4-17. https://doi.org/10.1109/JESTPE.2014.2319453

[5] Sprangle, Phillip, et al. "High-power lasers for directed-energy applications." *Applied optics* 54.31 (2015): F201-F209. https://doi.org/10.1364/AO.54.00F201
[6] Nored, Donald L. "Application of high power lasers to space power and propulsion." *2d NASA Conf. on Laser Energy Conversion*. 1976. https://ntrs.nasa.gov/citations/19760014427
[7] *The Atmospheric Window*, National Weather Service, https://www.weather.gov/jetstream/absorb. Accessed 23 Apr. 2022.
[8] Reine, M. B. "Photovoltaic detectors in MCT." *Infrared Detectors and Emitters: Materials and Devices* (2001): 313-376. https://doi.org/10.1007/978-1-4615-1607-1_12
[9] Blaser, Stephane, et al. "Free-space optical data link using Peltier-cooled quantum cascade laser." *Electronics Letters* 37.12 (2001): 778-780. https://doi.org/10.1049/el:20010504
[10] Liu, Jony J., et al. "Mid and long-wave infrared free-space optical communication." *Laser communication and propagation through the atmosphere and oceans VIII*. Vol. 11133. International Society for Optics and Photonics, 2019. https://doi.org/10.1117/12.2530969
[11] TheNoise. "p-n Junction at Equilibrium ." *Wikipedia*, 4 Aug. 2007, https://upload.wikimedia.org/wikipedia/commons/d/d6/Pn-junction-equilibrium.png. Accessed 23 Apr. 2022.
[12] "Detection of Light and Solar Cells." *Physics of Photonic Devices*, by Shun Lien. Chuang, John Wiley & Sons, 2009, pp. 764. https://dl.acm.org/doi/10.5555/1507539
[13] Hougen, C. A. "Model for infrared absorption and transmission of liquid-phase epitaxy HgCdTe." *Journal of Applied Physics* 66.8 (1989): 3763-3766. https://doi.org/10.1063/1.344038
[14] Moazzami, K., et al. "Detailed study of above bandgap optical absorption in HgCdTe." *Journal of electronic materials* 34.6 (2005): 773-778. https://doi.org/10.1007/s11664-005-0019-3
[15] Hansen, G. L., J. L. Schmit, and T. N. Casselman. "Energy gap versus alloy composition and temperature in Hg1− x Cd x Te." *Journal of Applied Physics* 53.10 (1982): 7099-7101. https://doi.org/10.1063/1.330018
[16] Hansen, G. L., and J. L. Schmit. "Calculation of intrinsic carrier concentration in Hg1− x CdxTe." *Journal of Applied Physics* 54.3 (1983): 1639-1640. https://doi.org/10.1063/1.332153
[17] Wenus, Jakub, Jaroslaw Rutkowski, and Antoni Rogalski. "Two-dimensional analysis of double-layer heterojunction HgCdTe photodiodes." *IEEE Transactions on Electron Devices* 48.7 (2001): 1326-1332. https://doi.org/10.1109/16.930647
[18] Clarke, Frederick W. "Nondestructive determination of free-electron concentration and mobility in Hg1− x Cd x Te, n-type InSb, and n-type GaAs." *Journal of applied physics* 75.9 (1994): 4319-4326. https://doi.org/10.1063/1.355974
[19] Mynbaev, K. D., and V. I. Ivanov-Omskiĭ. "Doping of epitaxial layers and heterostructures based on HgCdTe." *Semiconductors* 40.1 (2006): 1-21. https://doi.org/10.1134/S1063782606010015